On the scaling of jetting from bubble collapse at a liquid surface

Krishnan Sangeeth[1], E. J. Hopfinger[2] and Baburaj A. Puthenveettil[1]†

[1]Department of Applied Mechanics, Indian Institute of Technology Madras, Chennai- 600 036, India

[2]LEGI-CNRS-UJF, BP 53, 38041 Grenoble Cedex 9, France

(Received ?; revised ?; accepted ?. - To be entered by editorial office)

We present scaling laws for the jet velocity resulting from bubble collapse at a liquid surface which bring out the effects of gravity and viscosity. The present experiments conducted in the range of Bond numbers 0.004< Bo <2.5 and Ohnesorge numbers 0.001< Oh <0.1 were motivated by the discrepancy between previous experimental results and numerical simulations. We show here that the actual dependence of We on Bo is determined by the gravity dependency of the bubble immersion (cavity) depth which has no power law variation. The power law variation of the jet Weber number, $We \sim 1/\sqrt{Bo}$ suggested by Ghabache *et al.* (2014) is only a good approximation in a limited range of Bo values (0.1< Bo <1). Viscosity enters the jet velocity scaling in two ways: (a) through damping of precursor capillary waves which merge at the bubble base and weaken the pressure impulse, and (b) through direct viscous damping of the jet formation and dynamics. These damping processes are expressed by a dependence of the jet velocity on Ohnesorge number from which critical values of Oh are obtained for capillary wave damping, the onset of jet weakening, the absence of jetting and the absence of jet breakup into droplets.

Key words:

1. Introduction

Collapse of small bubbles at liquid surfaces is an ubiquitous phenomenon in nature. It is a fascinating fundamental problem because of the interconnection between capillary, gravity and viscous forces. The bubble breakup process at a free surface and the subsequent jetting was visualized first by Woodcock *et al.* (1953) using high speed photographic techniques who identified the following three stages: (i) the retraction and fragmentation of the top thin film, (ii) the collapse of the unstable cavity formed due to the absence of the thin film and (iii) formation and breakup of the jet. Kientzler *et al.* (1954) conducted experiments with a range of bubble sizes and found that the bubble collapse time decreases with decreasing bubble size. For small bubbles of radii less than 3 mm, it all happens in a time of the order of 10^2 to 10^3 μs with jet velocities of the order of 1 ms^{-1} to more than 10 ms^{-1}, when viscous damping can be neglected. This phenomenon is of importance in ocean- atmosphere exchange due to aerosol generation by fragmentation of thin film, which yields micro sized aerosol drops, and then by the jet

† Email address for correspondence: apbraj@iitm.ac.in

breakup, which produces larger sized droplets compared to those from film breakup, but still one order less than the bubble radius (Blanchard (1963); MacIntyre (1972); Spiel (1995); Lhuissier & Villermaux (2012)). In carbonated beverages like sparkling wine, small bubbles are desired because this enhances the aroma as was shown by Liger-Belair *et al.* (2012) for champagne. The aerosol generation by bubble bursting is found to be the mechanism behind the distinctive aroma (petrichor) after the first rain (Joung & Buie (2015)). Bubble bursting at a compound interface, like the interface formed after oil spill at the ocean surface, can lead to reverse mass transport of free surface materials into the bulk of the liquid (Feng *et al.* (2014)). In bio-reactors, bursting of free surface bubbles can cause mass scale bacterial cell destruction around aeration sites (Boulton-Stone & Blake (1993)). Recent studies by Shakhova *et al.* (2014) found that thawing of sub sea Arctic permafrost in East Siberia releases methane, a green house gas, and the transfer of this gas to the atmosphere is mediated by bubbles and its subsequent bursting at the ocean surface. The study reveals that bubbles, during stormy times, enhance the methane flux transfer from ocean to atmosphere. For all these reasons, this problem has received considerable attention so far.

A first attempt to understand the physics behind jetting from free surface bubble collapse was made by MacIntyre (1972) who conducted experiments with dyed bubbles, who proposed a boundary layer flow along the bubble cavity, which causes a stagnation pressure at the bottom of the cavity, causing jet formation. The bubble collapse at an air-water interface were first numerically simulated by Boulton-Stone & Blake (1993) (herein after BSB) for a range of bubble radii 0.5 mm $< R <$ 3 mm who then estimated the resulting jet velocities. Spiel (1995) measured the velocities of the first drops from air bubbles bursting at a water surface and proposed an empirical exponential dependence of jet velocity on R. A more comprehensive analysis of the scaling of jet velocities (U_j) was done by Duchemin *et al.* (2002), who performed direct numerical simulations for a wide range of sizes of air bubbles in water, 1.4μm $< R <$ 20 mm; they showed that $U_j/U_\mu \sim (R/R_\mu)^{-1/2}$, where $U_\mu = \sigma/\mu$ and $R_\mu = \mu^2/\rho\sigma$ are the viscous- capillary velocity and length scales with ρ being the liquid density, σ the liquid-gas surface tension and μ the dynamic viscosity. However, this dependence of U_j on R is not supported by the experimental results of Spiel (1995) nor the numerical simulations of BSB which are closer to $U_j \sim 1/R$ (Sangeeth *et al.* (2012)).

In order to answer this question of the dependence of jet velocity on bubble radius, and of the effects of viscosity and gravity on jet formation, experiments in other more viscous fluids and/or fluids of lower surface tension were needed. Such results, with different fluids, have recently been reported by Sangeeth *et al.* (2012) and Ghabache *et al.* (2014). Sangeeth *et al.* (2012) showed that, indeed, the viscous-capillary scaling ($U_j \sim 1/\sqrt{R}$) suggested by Duchemin *et al.* (2002) cannot collapse the experimental data, which displayed a $1/R$ variation for an intermediate range of R. Ghabache *et al.* (2014) showed that the gravity- capillary scaling, $We \propto Bo^{-1/2}$, ($U_j \sim 1/R$), collapse the data reasonably well for 0.007$< Bo <$1, where the jet Weber number $We = \rho U_j^2 R/\sigma$ and the Bond number $Bo = \rho g R^2/\sigma$, with g being the acceleration due to gravity. However, as we show in this paper, such a scaling is unlikely to hold for $Bo <$0.1 and $Bo >$1. Our data (see Sangeeth *et al.* (2012)) can also be approximated by a $Bo^{-1/2}$ dependence of We, but only for $0.1 < Bo < 1$, beyond which there are deviations from such a power law, as indicated also by the results of Spiel (1995) and BSB. In Ghabache *et al.* (2014), viscous effects were expressed as a dependence of $We\sqrt{Bo}$ on Morton number, $Mo = Bo\, Oh^4$, where Ohnesorge number $Oh = \mu/\sqrt{\rho R \sigma}$. However, the extremely small values of Mo in their scaling ($10^{-9} < Mo < 10^{-6}$) indicates the inadequacy of such a viscous scaling. These

	Water △ (20°C)	GW48 ▲ (30°C)	GW48 ▹ (20°C)	GW55 □ (20°C)	GW68 ∗ (30°C)	GW72 ◊ (30°C)	2-propanol + (20°C)	Ethanol ◃ (20°C)
μ mPa s	1.01	3.9	5.5	8	12.4	16.6	2.07	1.14
ρ kg m^{-3}	1000	1115	1120	1140	1170	1181	781	789
σ kg s^{-2}	0.072	0.068	0.068	0.067	0.066	0.064	0.018	0.022
R mm	0.18 - 4.08	0.42 -3.4	0.81-1.96	0.71 - 2.3	0.48 -2.3	0.6 - 3.6	1.46 - 2.41	0.19 - 1.16
Bo	0.004 - 2.27	0.029 -1.9	0.1 - 0.62	0.083 - 0.88	0.041 -0.89	0.063 - 2.36	0.9 - 2.4	0.013 - 0.47
$Oh \times 10^{-3}$	1.9 - 9	7.6 - 21.6	14 - 22	19.2 - 34.7	29.7 - 64.1	32 - 79.1	11.2 - 14.4	8 - 20
Re	2204 - 4276	774 -1506	627 - 723	284 - 393	19 -207	14 - 135	—	—

Table 1: Properties of the fluids, the range of radii of the bubbles and the range of dimensionless numbers used in the experiments. $Bo = \rho g R^2/\sigma$, $Oh = \mu/\sqrt{\sigma\rho R}$, $Re = \rho U_j R/\mu$.

issues called for further experiments and a search for the appropriate Bo dependence of the jet We and the possible limits of the $We \sim 1/\sqrt{Bo}$ "power law"; the scaling of viscous effects also needed reexamination.

In this paper we show that the Bo dependence of the jet We is closely related with the square of the dimensionless cavity depth, which implies that there is no simple power law scaling as proposed by Ghabache *et al.* (2014). We further show that the viscous damping effects are well captured by Ohnesorge number, for which critical values for capillary wave damping, dominant viscous damping, the absence of jet break up and the absence of jetting are given.

2. Experimental conditions

The experiments were conducted in a transparent acrylic tank of 3.5 × 5 cm^2 cross sectional area and in a glass tank of 5 × 5 cm^2 cross sectional area. The tanks were fixed on a leveling board and were filled up to the brim to avoid meniscus effects. We use distilled water and glycerol-water mixtures of 48%, 55%, 68 % and 72% glycerine concentration (herein after referred to as GW48, GW55, GW68 and GW72). In addition to these fluids, we have used 2-propanol and ethanol for the measurement of static parameters of the bubble, the properties of all these fluids are given in table 1. Gas bubbles in the range of equivalent spherical radii 0.17 mm $< R <$ 4.1 mm were produced by pumping air into glass capillary tubes of different sizes using a syringe pump operated at a constant discharge rate. The flow rate in the capillaries were selected so that the bubble detachment was within the periodic dripping regime described by Clanet & Lasheras (1999) and the periodic bubbling regime of Oguz & Prosperetti (1993). Care was taken to avoid crowding and merging of bubbles at the free surface. Capillaries were carefully fixed in the same alignment through out the experiments to avoid variations in bubble sizes (Doshi *et al.* (2003)). The liquids were changed after each run to minimize surface contamination.

The rising bubbles, which are almost elliptical in shape were photographed to determine the bubble volumes, from which the equivalent spherical radii R were calculated. The bubble stays at the free surface for a short time after its initial oscillations had died down and then bursts, giving rise to a vertical or nearly vertical jet. This time of stay for the smallest bubble of our experimentation (water, $Bo = 4.2 \times 10^{-3}$, $Oh = 9 \times 10^{-3}$) was 91 ms. The time of stay increased to more than 1 s with increasing Bo, i.e, beyond Bo=0.1, in water and GWs. Since the bubbles do not break during their

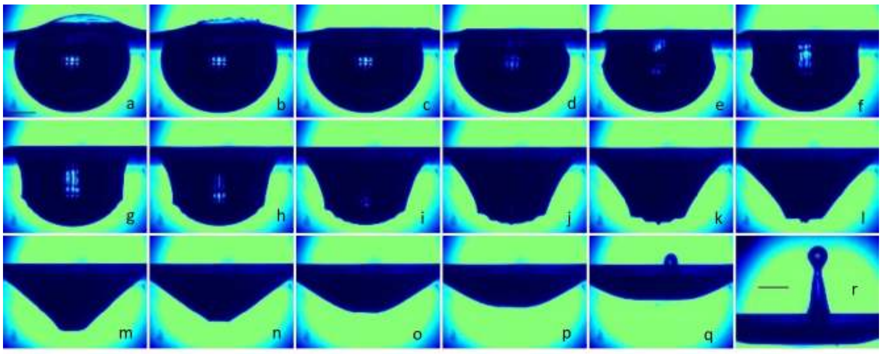

Figure 1: The bursting sequence of a bubble of radius R=2.15 mm, Bo=0.634, Oh = 0.00255 in water. Each image, from a to p, is separated by 0.25 ms. Images p to q and q to r are separated by 0.5 and 1.3 ms. The whole process up to jet emergence at the free surface took 4.5 ms. The lines in images a and r are 1 mm in length.

initial oscillations, possibly since the upper film is replenished; the bursting happens from a static configuration. This bursting process and the jet emergence from the free surface were captured by a high speed camera (La Vision ProHS for fps $\leqslant$19000 fps and Photron SA4 for fps $\leqslant$100000) using high intensity LED back lighting. The jet velocity was measured by tracking the tip of the jet in successive images, before the jet breaks up into drops. The image acquisition rates met the condition that $t_i < 1/\left|dU_j/dz\right|$, where t_i =1/fps. The spatial resolution was such that $\Delta Z_i < U_j\ t_e$, where ΔZ_i is the size of each pixel and t_e is the exposure time. The lowest and highest resolution for the imaging were 27μm/pix and 3.4μm/pix. The corresponding jet diameters are 1.3mm and 0.03mm respectively; the jets were hence well resolved in our images. For glycerol- water mixtures, the viscosity values are less sensitive to changes in temperature at 30^{0}C than at 20^{0}C; i.e, $(\partial\mu/\partial T)_{20^0C} > (\partial\mu/\partial T)_{30^0C}$. Hence, in regimes where viscosity of the jet is strongly dependent on viscosity (or Oh), especially when sharp changes in velocity is expected with change in Oh, like at Oh = 0.037 where the viscous cut off occurs, we conducted experiments at 30^{0}C so that small changes from the set temperatures do not change the viscosity much. The experiments were conducted in a temperature controlled laboratory after the temperature stabilised to the set values of 20^{0}C or 30^{0}C.

3. Jet velocity scaling

A typical bubble collapse sequence is shown in figure 1 for a bubble of R = 2.15 mm in water. Time evolution of the jets for the same and other conditions are shown in Figures B.15 and B.16 in Appendix B. Note that there are precursor capillary waves ahead of the kink caused by the change of the curvature of the bubble boundary from convex to concave, as seen in images f to k in figure 1. The group velocity of these waves is equal to the kink velocity as is observed ahead of the crest of steep water waves (Perlin *et al.* (1993)). These dispersive capillary waves, cause perturbations and hence weaken the jet velocity either through a weakening of the pressure impulse at the base or by bubble pinch-off. In the coalescence of larger bubbles, bubble pinch-off is a frequent phenomenon (Zhang & Thoroddsen (2008), Zhang *et al.* (2015)). However, here bubble

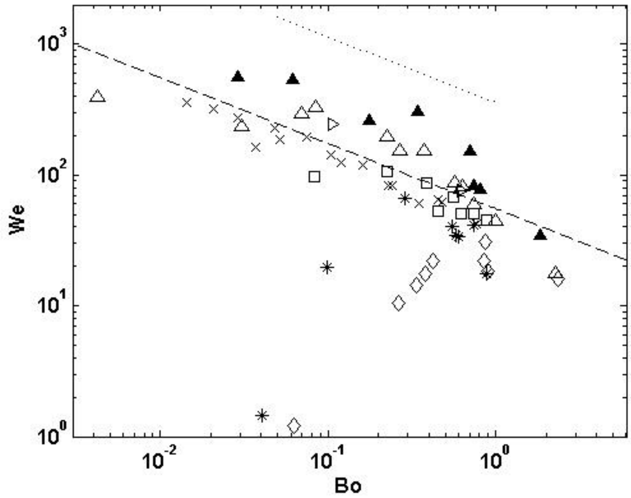

Figure 2: Weber number of the emerging jet velocities as a function of the Bond number. $\triangle$, Water; $\blacktriangle$, GW48 (30°C); $\triangleright$, GW48 (20°C); $\square$, GW55; $*$, GW68; $\diamond$, GW72; $\times$, Ghabache *et al.* (2014)'s jet velocities for water; - -, $We = 55Bo^{-1/2}$; ..., Ghabache *et al.* (2014)'s jet velocities for GW of viscosities 4.4 to 6.2 mPas.

pinch-off is very rare. With decreasing bubble size or with increasing viscosity these capillary waves are progressively damped, giving rise to an increase in jet velocity. The question of capillary wave damping and its effect on jet velocity will be examined in §3.2; we focus first on the question of the origin of gravity effects on jet velocity.

3.1. *Gravity effects*

Figure 2 shows the square of the dimensionless jet velocity $(U_j/U_c)^2 = We$, versus the square of the dimensionless radius $(R/R_c)^2 = Bo$, where the capillary velocity, $U_c = \sqrt{\sigma/\rho R}$ and the capillary radius, $R_c = \sqrt{\sigma/\rho g}$. The water data of Ghabache *et al.* (2014) are included in figure 2 for comparison and their results with GW of 4.4 to 6.2 times the water viscosity are indicated by the dotted line. The jet velocities of Ghabache *et al.* (2014) in GW is larger with respect to that in water by about a factor of 2; we do not observe such a large velocity increase in GW48. When capillary waves are damped the bubble boundary is smoother and this may lead to a higher impulse at the bubble base and hence a higher jet velocity. Furthermore, it is clear from figure 2 that Ghabache *et al.* (2014) data show a good correlation of We with $Bo^{-1/2}$ ($1/R$ variation) as shown by the dashed line, which shows

$$We = 55\ Bo^{-1/2} \tag{3.1}$$

over the whole range of Bo considered. At a first view, our experimental results also seem to support a $1/R$ variation of the jet velocity except when viscous effects become important, on the bubble scale, as is in the case of GW68 and GW72. However, there is a deviation in our data from the $1/R$ behaviour when $Bo > 1$, and furthermore, there is a deviation of We from the $Bo^{-1/2}$ dependence when $Bo < 0.1$, with the trend of We becoming independent of Bo. Even in the range $0.1 < Bo < 1$ we, in fact, show later that the $Bo^{-1/2}$ scaling is only a good approximation and a continually varying power of Bo fits the present data, as well as those of Spiel (1995) and BSB, better. We also

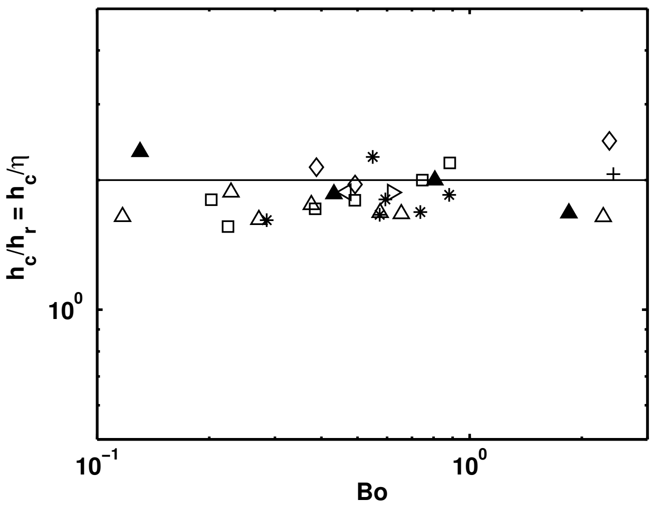

Figure 3: $h_c/h_r = h_c/\eta$ as a function of Bo. $\triangle$, Water; $\triangleright$, GW48 (20^{o}C); $\blacktriangle$, GW48 (30^{o}C); $*$, GW68; $\Diamond$, GW72; $\triangleleft$, ethanol; $+$, 2-propanol; —, $h_c/h_r = 2$.

note from figure 2 that We at the same Bo first increase with increase in viscosity (see water and GW48) and then decrease monotonically with a further increase in viscosity; we discuss this viscosity effect in § 3.2.

The question is, what is the reason for the gravity (Bo) dependence of jet Weber number and why should there be a $Bo^{-1/2}$ dependence? It is well known that the jet velocity resulting from cavity collapse related with stationary surface gravity waves depends on the cavity depth or last wave amplitude (Zeff *et al.* (2000); Das & Hopfinger (2008)). We expect a similar association between jet velocity and bubble cavity depth in the case of bubble collapse. In bubble collapse, the cavity depth is determined by the balance between gravity and surface tension forces, as will be shown below.

3.1.1. *Dimensionless cavity depth*

The cavity depth Z_c is defined as the depth of the base of the bubble from the free, undisturbed, liquid surface. A theoretical expression of Z_c can easily be obtained when neglecting bubble deformation. To leading order,

$$Z_c = 2R - h_c, \tag{3.2}$$

where h_c is the height of the top of the bubble from the free surface (see inset of figure 4). Assuming symmetry at the point of inflection of the bubble surface at the rim gives,

$$h_c = 2\eta, \tag{3.3}$$

where $\eta = h_c - h_r$ is the height of the bubble cap above the rim, with h_r being the height of the rim from the free surface. Figure 3 shows $h_c/h_r = h_c/\eta$, plotted against Bo in the range $10^{-1} < Bo < 3$. The measured values are close to $h_c/h_r = h_c/\eta = 2$, hence the validity of the assumptions leading to (3.3) is supported by experiments. The relatively large experimental error is due to the very small values of h_r and h_c.

For a spherical bubble, from geometry,

$$\eta = R - \sqrt{R^2 - R_r^2}, \tag{3.4}$$

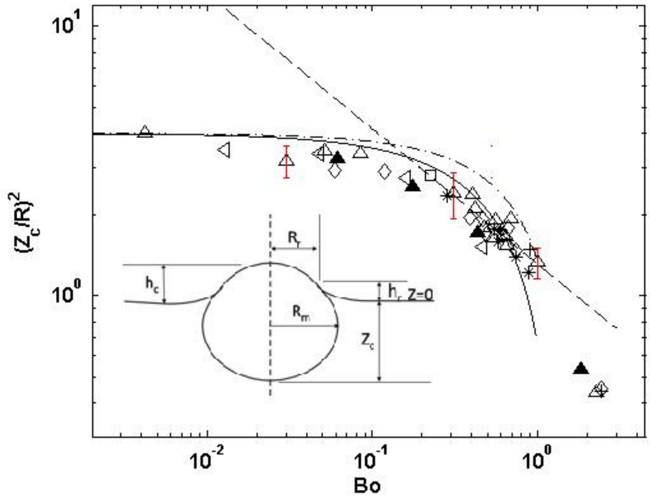

Figure 4: Square of the dimensionless cavity depth of the bubble as a function of the Bond number. △, Water; ▷, GW48 (20^0C); ▲, GW48 (30^0C); ∗, GW68; ◊, GW72; ◁, ethanol; +, 2-propanol; - -, $1.32Bo^{-1/2}$; -.-, $(Z_c/R)^2 = 4(1-2/3Bo)$; —,$(Z_{cd}/R)^2 = 4(\sqrt{1-2/3Bo} - 0.17Bo^{0.8})^2$.

where R_r is the radius of the rim (figure 4). From the force balance, $F_B = F_\sigma$, where the buoyancy force, $F_B = \rho g(4/3)\pi R^3(1-\eta^2(3-\eta/R)/4R^2)$ and the surface tension force, $F_\sigma = (2\sigma/R)\pi R_r^2$, we get

$$\frac{R_r}{R} = \sqrt{\frac{2}{3}Bo(1-\frac{\eta^2}{4R^2}(3-\frac{\eta}{R}))}. \tag{3.5}$$

When $Bo \leqslant 1$, $\eta/R \leqslant 0.4$, so the term $\eta^2(3-\eta/R)/4R^2 \leqslant 0.1$, which can be neglected to first order, resulting in,

$$\frac{R_r}{R} \simeq \sqrt{\frac{2}{3}Bo}, \tag{3.6}$$

which when substituted in (3.4) gives,

$$\eta = R(1-\sqrt{1-\frac{2}{3}Bo}). \tag{3.7}$$

Using (3.7) in (3.3), we get from (3.2),

$$\frac{Z_c}{R} = 2\sqrt{1-\frac{2}{3}Bo}. \tag{3.8}$$

Figure 4 shows the square of the experimental $(Z_{ce}/R)^2$ and the theoretical dimensionless cavity depths $(Z_c/R)^2$ as a function of Bo. Note that we plot $(Z_c/R)^2$ rather than Z_c/R because the Weber number also has the square of velocity. It is seen that in the range $0.1 < Bo < 1$, the experimental (Z_{ce}/R) can be fitted by $(Z_{ce}/R)^2 \sim Bo^{-1/2}$ which is the same approximate dependence of We on Bo seen in figure 2. In figure 2, when Bo is large, $Bo > 1$, the jet velocity starts to decrease and at $Bo = 2.25$, $R = 4.08$ mm in water, We deviates considerably from the $Bo^{-1/2}$ correlation. The experimental $(Z_{ce}/R)^2$ in figure 4 shows a similar deviation from the approximate power law $Bo^{-1/2}$.

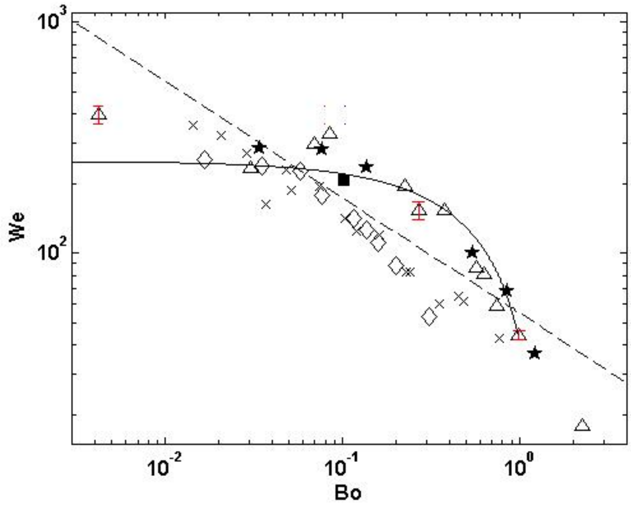

Figure 5: Variation of jet Weber number with Bond number in water. △, present experiments; ★, BSB; ◇, Spiel (1995), drop velocities; ■, Kientzler *et al.* (1954); — , $We = 62.5\ (Z_{cd}/R)^2$; - -, $We = 55Bo^{-1/2}$; ×, Ghabache *et al.* (2014)'s jet velocities for water.

The theoretical $(Z_c/R)^2$ has a steeper fall off with Bo than the experimental $(Z_{ce}/R)^2$ because when $Bo > 1$, the limit of validity of (3.8) is approached. When $Bo \to 0$ the cavity depth tends to the asymptotic limit of $2R$ and is practically independent of Bo when $Bo < 0.1$ because for $Bo = 0.1$, $Z_c/R = 1.93$ and for $Bo = 0.01$, $Z_c/R = 1.99$, which is only a 3 % variation. We can therefore assume that when $Bo < 0.1$, Z_c/R is nearly invariant. On the other hand, between $Bo = 0.1$ ($Z_c/R = 1.93$) and $Bo = 1$ ($Z_c/R = 1.15$) gravity has a large effect on the cavity depth.

The bubble deformation is negligible up to $Bo \approx 0.1$ and remains small up to $Bo \approx 3/2$, with the deformation varying from about 4 to 15 % of R as Bo increases from 0.1 to 1. Although these deformations are relatively small this seems to affect the cavity depth sufficiently when $Bo < 1$ to make the theoretical depths (3.8) deviate noticeably from the experiments as can be seen in figure 4 when $Bo < 1$. Z_c/R given by (3.8) can be corrected for these small deformations by assuming an ellipsoidal shape of the bubble. The expression for such a corrected cavity depth is $Z_{cd}/R \approx 2(R/R_m - 1 + \sqrt{1-(2/3)Bo})$, where R_m is the measured horizontal radius at the equator, approximated by $R/R_m \approx 1 - 0.17Bo^{0.8}$, to get,

$$\frac{Z_{cd}}{R} = 2\left(\sqrt{1 - \frac{2}{3}Bo} - 0.17Bo^{0.8}\right). \qquad (3.9)$$

As shown by the continuous line in figure 4, we obtain a better match of $(Z_{cd}/R)^2$ vs Bo obtained from (3.9), with the experimental variation of $(Z_{ce}/R)^2$ vs Bo.

Gravity effects can be best demonstrated with data from one fluid alone rather than data from different viscosity fluids as in figure 2. Figure 5 shows the experimental jet velocities for water plotted in terms of We vs Bo, along with the data from BSB, the drop velocities measured by Spiel (1995), the jet velocity measured from the images of Kientzler *et al.* (1954) and the jet velocity data of Ghabache *et al.* (2014). The continuous

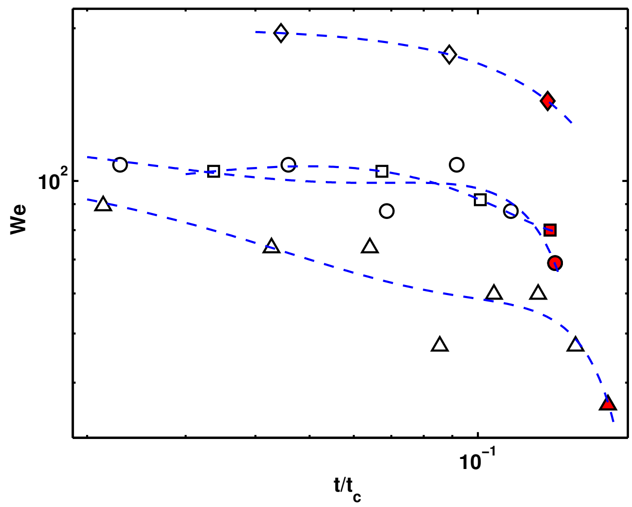

Figure 6: Variation of jet We with dimensionless time for bubbles of different Bo in water. $\diamond$,$Bo = 0.2$; $\Box$, $Bo = 0.3$; $\circ$, $Bo = 0.49$; $\triangle$, $Bo = 0.63$. Unfragmented jet velocities are shown by hollow symbols while the velocities of the first drop after jet fragmentation are shown by filled symbols. The lines which are cubic polynomial fit show the progression of velocities with time or height of each jet.

line is

$$We = 62.5 \left(\frac{Z_{cd}}{R}\right)^2 \tag{3.10}$$

while the dashed line is (3.1). The following three regimes could be identified in figure 5.

(*a*) $Bo < 0.1$: At these low Bo numbers the theoretical cavity depth varies only by 3% from $Bo = 0$ to 0.1 (see figure 4) and according to the model We should also asymptote to a constant value, as shown by the solid line in figure 5. Our data and those of BSB tend to asymptote toward such a constant value of We rather than to increasing We with decreasing Bo, following a $Bo^{-1/2}$ law, given by Ghabache et al. The deviation of our data from the cavity depth model, seen as a slight increase in We with decreasing Bo, for $Bo < 0.1$ is due to capillary wave damping. As we discuss in § 3.2, if the Weber number is corrected for this damping, the corrected We is practically a constant for $Bo < 0.1$.

(*b*) $Bo > 1$: In this range, there is, no doubt, a clear deviation of our We data from the $Bo^{-1/2}$ trend. This is because the cavity depth decreases more rapidly with Bo than $Bo^{-1/2}$ and there is also larger bubble deformation for $Bo > 1$. Here also, Ghabache et al does not have data at $Bo > 1$ to see the deviation from the $Bo^{-1/2}$ trend.

(*c*) Intermediate range $0.1 < Bo < 1$: In this range, there is a fairly large dispersion of the data. Ghabache et al's data are well fitted by $Bo^{-1/2}$ whereas the present results and those of BSB deviate noticeably from this power law. The results of BSB closely follow the cavity depth model. For $0.06 < Bo < 0.15$ Spiel's results follow $We \sim Bo^{-1/2}$ but deviate from this power law when Bo increases. Spiel measured the first drop velocities and not the jet tip velocities when the jet emerges from the free surface; the values of the drop velocities could be different from the unbroken jet tip velocities. Figure 6 shows the measured jet velocities at increasing heights as time increases, culminating in the first drop velocity due to jet fragmentation at some height. We see that at moderate Bo

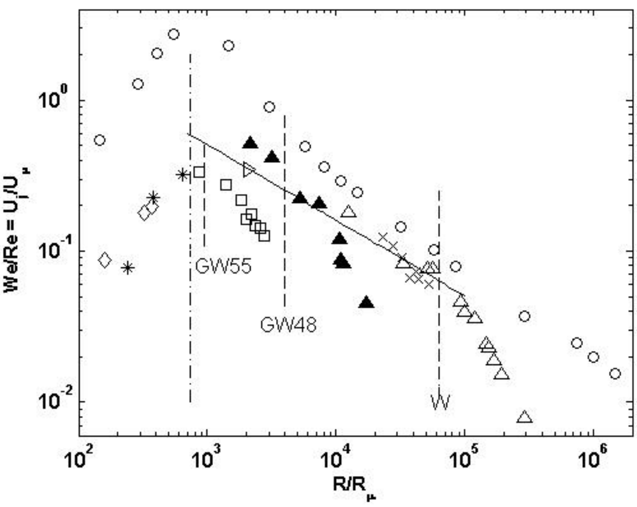

Figure 7: Variation of the dimensionless jet velocity with the dimensionless bubble radius for low Bo. The velocities and radii are normalised by the viscous capillary scales: $\triangle$, Water; ▲, GW48 (30^{o}C); ▷, GW48 (20^{o}C); □, GW55; $*$, GW68; ◇, GW72; ◯, Duchemin *et al.* (2002) jet velocities for water; $\times$, Ghabache *et al.* (2014) jet velocities for water; —, $16(R/R_\mu)^{-1/2}$; -.-, the viscous cut off at $R/R_\mu = Oh^{-2} \simeq 730$; - -, the vertical dashed lines demarcate the $Bo < 0.1$ data on the left with the $Bo > 0.1$ data on the right for water (W), GW48 and GW55. Viscous- capillary scaling is seen for $Bo < 0.1$ part of each data set.

($0.2 \leqslant Bo \leqslant 0.63$) there is a 30% to 60% reduction in drop velocity compared to the jet velocity at the free surface. This reduction in drop velocities increases with increasing Bo since jets from larger Bo bubbles fragment farther away from the free surface. This decrease in drop velocities at moderate Bo is the reason why Spiel's data is lower than the solid curve from the cavity model in figure 5.

Based on the above considerations, we hence conclude that the present experimental data for water and BSB data, when considered over the whole range of Bo, show better agreement with (3.10) than with (3.1). This leads us to the important understanding that the gravity effects on the jet velocity, leaving aside the viscosity effects, have the same functional dependence as the gravity effects on the cavity depth of the bubble, which, given by (3.9), does not follow a $Bo^{-1/2}$ power law. It could be argued that the dynamic cavity depth when the singular collapse commences (figure 1 m) is of importance and not the static depth just after the surface film disintegration (figure 1 c). An estimate of the change in cavity depth during the time of bubble collapse $t_{bc} \approx 0.3\ t_c$ (Sangeeth & Puthenveettil (2015)), where the capillary time $t_c = R\sqrt{\rho R/\sigma}$ is obtained by evaluating the upward bubble displacement $\Delta z = g t_{bc}^2/2$ to get,

$$\Delta z/R \approx 4.5 \times 10^{-2} Bo, \tag{3.11}$$

which is negligible when $Bo < 1$. Any decrease in cavity depth would hence have to be due to capillary forces caused by the curvature of the bubble base, our experiments show that this is small for small bubble sizes.

The proposed scaling law for gravitational effects on jet velocity, namely $We \sim (Z_{cd}/R)^2$, where Z_{cd}/R is given by (3.9), implies that the jet We becomes practically independent of Bo at $Bo < 0.1$. Hence at these low Bond numbers the viscous-capillary scaling of Duchemin *et al.* (2002) should be appropriate. As shown in figure 7, the data closely follow the relation

$$\frac{U_j}{U_\mu} = 16\left(\frac{R}{R_\mu}\right)^{-1/2} \tag{3.12}$$

for $Bo < 0.1$. This power law variation of jet velocity gives $U_j = 16\ U_c$ or $We = (U_j/U_c)^2 \simeq 250$ as seen in figure 5 for $Bo < 0.1$. The relation (3.12) implies that $U_j \sim 1/\sqrt{R}$ (Duchemin *et al.* (2002)). Curiously their data deviate from the $R^{-1/2}$ scaling when $R/R_\mu < 5 \times 10^3$, which is not observed in the present experiments. The data of Ghabache *et al.* (2014) show a $We \sim Bo^{-1/2}$ scaling for their whole range of Bo, $0.007 < Bo < 1$.

3.2. *Viscosity effects*

Ghabache *et al.* (2014) expressed the viscosity dependence of jet velocity by plotting $We\sqrt{Bo}$ in terms of Morton number $Mo = Oh^4 Bo$, a dimensionless number that contains gravity. However, there is no physical reason as to why gravity should be important in viscous damping of capillary driven flows. Gravity determines the cavity depth and shape, but once formed, the collapse, after film rupture, is surface tension driven; as indicated above, the change in cavity depth in the bubble collapse time due to gravity is negligibly small when Bo is of order one or less. The importance of viscous effects on capillary driven flows is therefore expressed by an Ohnesorge number which is the ratio of viscous to capillary forces.

Viscosity enters the jet velocity scaling in two ways: (a) through damping of the capillary waves which merge at the bubble base and weaken the pressure impulse and (b) through direct viscous damping of the jet formation and dynamics. Figure 8 shows the damping of capillary waves on the collapsing cavity surface with increase in Oh. Figure 8 (*a*)-(*b*) is a bubble collapse sequence of a moderate Bo water bubble ($Bo = 0.63$) with $Oh = 0.0026$. Here, in the wave train preceding the kink two wavelengths $\lambda_1 \approx 0.36R$ and $\lambda_2 \approx 0.17R$ can be clearly identified, with faster and shorter waves being practically damped. The wave train, group velocity $C_g = 3/2\ \sqrt{\sigma\ k/\rho} \simeq 3/2\ \sqrt{2\pi\sigma/\rho\lambda_1} \approx 6\ U_c$ which corresponds to the measured speed of the kink. Figure 8 (*c*) -(*d*) is a collapsing sequence of a smaller water bubble ($Bo = 3 \times 10^{-2}$) with a relatively larger $Oh = 0.0055$ which shows only wavelength λ_1 clearly; the shortest wave (λ_2) is nearly damped. Figure 8 (*e*)-(*f*) show the capillary waves in GW48 (30^0C) bubble with $Oh = 0.0139$ in which the longer wave (λ_1) alone moves ahead of the kink, with the amplitude noticeably decreased. As can be seen in figure 8 (*g*)-(*h*), a further increase in Oh from 0.0139 to 0.0225 results in complete damping of the capillary waves on the cavity surface.

The amplitude α of capillary waves falls off exponentially in the form $\alpha = \alpha_0 e^{-\kappa t}$ with the damping rate $\kappa = 8\pi^2\mu/\rho\lambda^2$. In the collapse time $t_{bc} \approx 0.3 t_c$ (Sangeeth & Puthenveettil (2015)), the decrease in capillary wave amplitude is given by

$$ln\Big(\frac{\alpha}{\alpha_0}\Big) \approx -24\Big(\frac{R}{\lambda}\Big)^2 Oh. \tag{3.13}$$

Capillary waves can be considered completely absent when $\alpha/\alpha_0 = e^{-n}$ with $n \approx 4$. Equation (3.13) with $n = 4$ then implies that capillary waves with wave length less than $\lambda/R \approx 0.17$ are absent at a value of $Oh \approx 0.0048$ (see figure 8 (a) to (d)). Similarly, capillary waves of wave length less than $\lambda/R \approx 0.36$ will be absent at $Oh \approx 0.022$ (see figure 8 (e) to (h)). We can hence infer that capillary waves are progressively damped as Oh increases and there is an increase in jet velocity up to about $Oh \approx 0.02$ due to this.

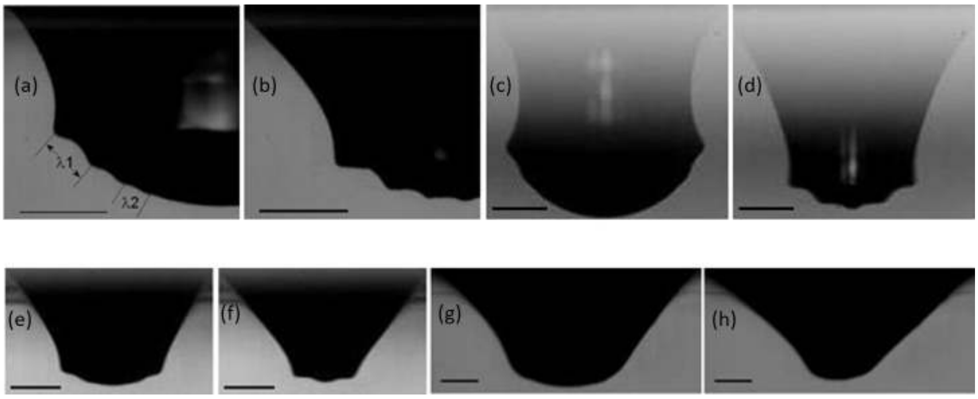

Figure 8: Progressive damping of capillary waves with increase in Oh, shown in image pairs from (a) to (h). Collapsing sequence, (a)-(b): water, $Oh = 0.0026$ ($Bo = 0.63$); (c)- (d): water, $Oh = 0.0055$ ($Bo = 3 \times 10^{-2}$); (e)-(f): GW48 (30^0C), $Oh = 0.0139$ ($Bo = 0.17$); (g)-(h): GW55, $Oh = 0.0225$ ($Bo = 0.47$). In each image pair, images are separated by 741, 100, 148 and 375 micro seconds, respectively. The line in (a)-(b): 1mm, (c)- (d): 0.2mm, (e)-(f): 0.5mm, (g)-(h):0.5mm.

An increase in Oh could occur due to decrease in bubble radius resulting in a corresponding decrease in Bo. We saw in figure 5 that with decrease in Bo for $Bo < 0.1$, the jet We increases, deviating from the cavity model (3.10). We can now understand that such a deviation is an effect of viscosity since precursor capillary waves are more and more damped by viscosity as the bubble radius gets smaller leading to an increase in jet velocity due to a smoother cavity. We assume that there is a dependence of We on Oh in the form $Oh^{1/2}$, same as that of λ/R from (3.13), due to capillary wave damping with increase in Oh. If the Weber number is now corrected for this damping by normalising with $Oh^{1/2}$, as shown in figure 9, $We/Oh^{1/2}$ is practically a constant for $Bo < 0.1$. Spiel's We is also practically independent of Bo when $Bo < 0.06$. Even Ghabache's data could be considered to be following our cavity depth model in figure 9. Unfortunately, Ghabache et al. have no measurements at smaller Bo, say at Bo about 0.003 for a clearer verification.

In figure 10 we have plotted $We/(Z_{cd}/R)^2$ as a function of Ohnesorge number, Oh. It is seen that when $Oh > Oh_c \simeq 0.037$ there is a rapid decrease in jet velocity since viscous effects become important in jetting. Corresponding to Oh_c, we can estimate a critical Bond number $Bo_c = \mu^4 g/(0.037)^4\sigma^3\rho$, which is 1.5×10^{-5} in water, beyond the range of our experiments. For higher viscosity fluids like GW68 and GW72, $Bo_c = 0.3$ and $Bo_c = 1.28$ respectively, which could be seen in figure 2, where a rapid drop of We occurs for $Bo < Bo_c$.

When $Oh < Oh_c$, except in the range of $0.02 < Oh < Oh_c$, the data sets of water and GW48 indicate an increase of $We/(Z_{cd})^2$ with Oh in figure 10. There is also a small region of decreasing $We/(Z_{cd})^2$ with Oh at small Oh, which is an artefact of the deviation of the theoretical cavity depth from the experimental values at large Bo (see figure 4). In addition, the GW48 data (filled triangles) have larger We values compared with that of water. As mentioned above, this increase of $We/(Z_{cd})^2$ with Oh occur because capillary waves are more and more damped as Oh increases, leading to a smoother cavity and hence a stronger pressure impulse. Hence, in figure 10, we plot the compensated We,

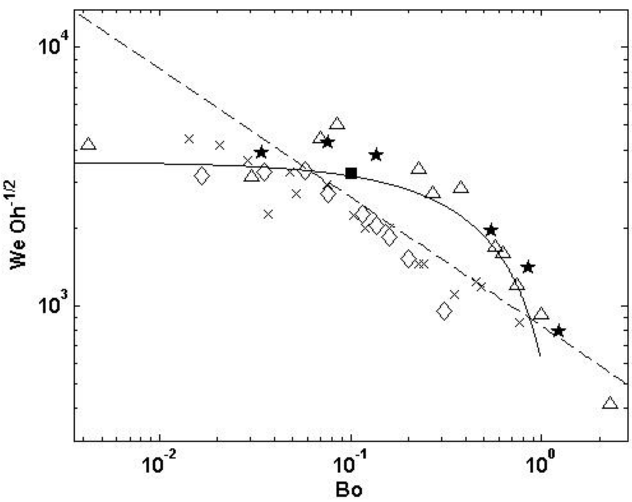

Figure 9: Variation of Weber compensated for capillary wave damping with Bo. Symbols are the same as in Figure 1. - -, $WeOh^{-1/2} = 830\ Bo^{-1/2}$; —, $WeOh^{-1/2} = 900(Z_{cd}/R)^2$.

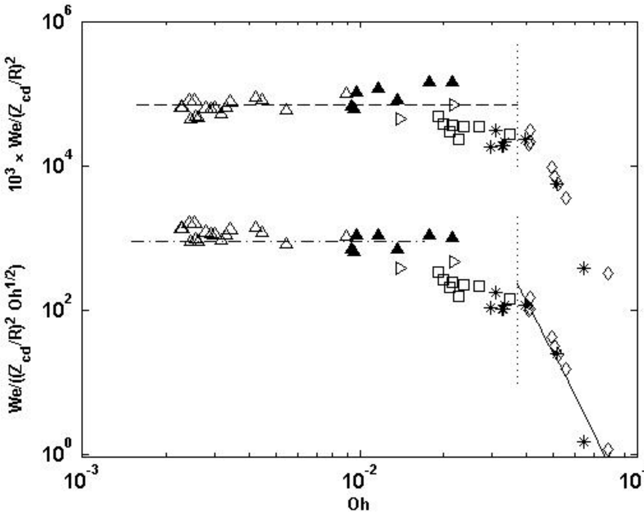

Figure 10: $10^3 \times We/(Z_{cd}/R)^2$ and $We/\left((Z_{cd}/R)^2 Oh^{1/2}\right)$ as functions of $Oh = \mu/\sqrt{\sigma\rho R}$. $\triangle$, Water; $\blacktriangle$, GW48 (30^{o}C); $\triangleright$, GW48 (20^{o}C); $\square$, GW55; $*$, GW68; $\Diamond$, GW72; $\times$, water data of Ghabache *et al.* (2014); - -, $We/(Z_{cd}/R)^2 = 70$; -.-, $We/\left((Z_{cd}/R)^2 Oh^{1/2}\right) = 900$; —, $We/((Z_{cd}/R)^2 Oh^{1/2}) = 8.3\times10^{-9} Oh^{-7.3} - 0.17$; ..., the vertical dotted line represents Oh_c=0.037.

$We/((Z_{cd}/R)^2 Oh^{1/2})$ as a function of Oh. This rescaling collapse the present water and GW48 data reasonably well to a nearly constant value of compensated We. The increase in compensated We with decrease in Oh at small Oh (large Bo) still persists, being an outcome of (3.9) being valid only till $Bo \approx 1$; a relation valid for $Bo > 1$ would remove this trend.

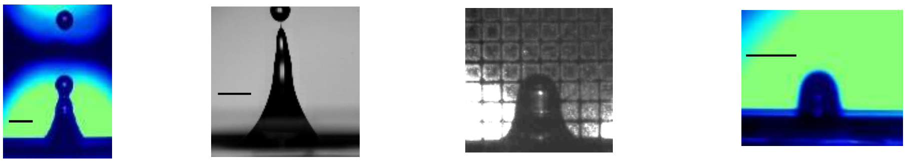

(a) (b) (c) (d)

Figure 11: Images of jets for different conditions giving an idea of the effect of Bond number and viscosity. (a) Bubble of R= 2.15 mm in water, Bo= 0.629, Oh= 2.55 $\times$ 10^{-3}; (b) R= 2 mm in GW48 (30^{o}C), Bo= 0.646, Oh= 10 $\times$ 10^{-3}; (c) R=4.08 mm in water, Bo= 2.25, Oh= 1.85 $\times$ 10^{-3}; (d) R= 1.46 mm in GW72, Bo= 0.39, Oh= 4.9 $\times$ 10^{-2}. The lines in images 11a, 11b and 11d are 1 mm in length. The grid size in image 11c is 1 mm.

Figure 10 clearly indicates the existence of an intermediary regime in the range $0.02 < Oh < Oh_c$ where the compensated Weber number falls below the nearly constant value observed when $Oh < 0.02$. This reduction in jet velocity is most likely due to a viscous effect on the jet scale expressed here by the jet Reynolds number $Re = \rho U_j R/\mu$ that decreases from about 10^3 in the case of GW48 to 10^2 for GW55 (see table 1). For the latter experiment, when Re is defined with the jet radius instead the bubble radius, it is well below 10^2.

When $Oh > Oh_c$ the Reynolds number on the bubble scale falls below 10^2 and the jet velocity decreases rapidly with increasing Oh. Note that $Oh_c = 0.037$ corresponds to $R/R_\mu = Oh^{-2} \simeq 730$ in figure 7, below which the jet velocity drops off rapidly in agreement with the numerical simulations of Duchemin *et al.* (2002). In figure 10 we have empirically fitted this viscous regime by $We/((Z_{cd}/R)^2 Oh^{1/2}) = 8.3\times10^{-9} Oh^{-7.3} - 0.17$. This critical value above which the jet velocity decreases rapidly corresponds to the value proposed by Walls *et al.* (2015) as a critical value beyond which the jet does not break up into drops. Figure 9 shows images of jets for different Oh values. It is seen that for conditions of figure 11d, $Oh = 0.05 > Oh_c$, for instance, there is no breakup of the jet into drops (figure B.16d), whereas breakup occurs for lower values of Oh (figure 11a to 11b). In figure 11c there is no breakup either, even though $Oh < Oh_c$ (see figure B.15a for full sequence of jet evolution). This is because Bo is large, as discussed below in § 3.2.1. Furthermore, we find that no jet emerges when $Oh = Oh^* \simeq 0.1$, a value larger than the value of $Oh^* = 0.052$ proposed by San Lee *et al.* (2011). The difference could possibly arise from the small liquid layer depth (of the order of R) in their experiments.

3.2.1. *Large Bond number*

At very large Bo numbers, the ascending velocity of the bubble due to the buoyancy force approaches the bubble collapse velocity due to the capillary force. An estimate of Bo for no jet formation can be obtained from (3.11) by using $\Delta z \approx 0.5\ R$ during the collapse time to obtain $Bo \approx 12$. Walls *et al.* (2015) indicate that there is still jet formation at $Bo \approx 5$ (bubble in water) but no breakup into drops. As seen in figure 11c, our experiments also show no drop formation for a $R = 4.08$ mm bubble in water at $Bo = 2.25$. Hence we expect that at $Bo \approx 10$ no jet will be formed.

4. Conclusions

The first main novel result from the present work is that the dependence of the dimensionless jet velocity, expressed in terms of the Weber number (We), on the Bond number (Bo) is determined by the dimensionless cavity depth. The variation of the square of the dimensionless cavity depth $(Z_{cd}/R)^2$ of the bubble with the Bond number is of the same form as that of the We with Bo (compare figures 4 and 5), which is not a power law. In a limited range of Bond number values, $0.1 < Bo < 1$, this dependence can however be approximated as $Bo^{-1/2}$ as was proposed by Ghabache *et al.* (2014). When $Bo < 0.1$ the cavity depth approaches the asymptotic limit of $Z_c/R \simeq 2$ and is practically independent of Bo; the viscous-capillary scaling of Duchemin *et al.* (2002) is then appropriate (figure 7). In the large Bond number limit ($Bo > 1$) the cavity depth decreases rapidly and so does the jet velocity or We. Bubble deformation also becomes important at these large Bo numbers. No approximate power law for We in terms of Bo exists when $Bo > 1$.

The second important conclusion is that viscosity effects are best expressed in terms of Ohnersorge number (Oh=viscous/capillary forces), which is usual for capillary driven flows. Jet formation is strongly affected by viscosity when $Oh > Oh_c \simeq 0.037$ with the jet formation being completely inhibited when $Oh = Oh^* \simeq 0.1$. In the range $Oh < 0.02$ an increasing viscosity can increase the jet velocity through capillary wave damping; the present experiments suggest that We is proportional to $\sqrt{Oh}$ in this regime. In the intermediate range $0.02 < Oh < Oh_c$ jet velocities are lower because of low jet Reynolds number. When $Oh > Oh_c$ the Reynolds number is also small on the bubble scale.

While the present results are in overall agreement with those of Ghabache *et al.* (2014), we point out important differences which exist at small Bond numbers ($Bo < 0.1$) and large Bond numbers ($Bo > 1$). These differences occur due to the variation of the cavity depth with Bo, which deviates from the approximate $Bo^{-1/2}$ power law at small and large Bo. In addition, we bring out the complex effects of viscosity, which result in three regimes, the first in which viscosity affects the jet dynamics at large Oh, the second in which it affects only the jet formation and finally the third regime in which viscosity affects the jet velocity through capillary wave damping.

We are grateful to Prof. Mahesh Panchagnula, Dept. of Applied Mechanics, IIT Madras, for allowing us to use the high speed photographic facility in his lab.

Appendix A. Jet velocity and cavity depth

The relation of jet velocity with cavity depth can also be demonstrated by considering that the jet velocity is given by

$$U_{jc} = \widetilde{Z}_{cd}/t_j, \tag{A 1}$$

where t_j is the time measured from the beginning of vertical retraction of the conically shaped cavity (figure 1m) to jet emergence at the free surface (just before figure 1q) and $\widetilde{Z}_{cd}$ is the cavity depth at the instant when the conically shaped cavity starts to retract vertically (see figure A.12). In writing equation (A 1), it is assumed that the jet velocity inside the cavity is constant and that the impulse at the conical cavity bottom occurs in a time short compared with t_j. As shown in figure A.13a, $\widetilde{Z}_{cd}$ is found to be directly proportional to Z_{cd} with no additional dependence on Bo so that,

$$\widetilde{Z}_{cd} = C_1 Z_{cd}, \tag{A 2}$$

where, from measurements in water,$C_1 = 0.86$. The measured values of t_j scales with the capillary time, $t_c = \sqrt{\rho R^3/\sigma}$ as,

$$t_j = C_2 t_c. \tag{A 3}$$

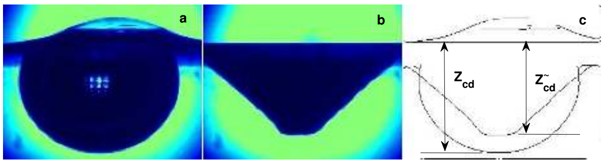

Figure A.12: (a) Static bubble of $R = 2.15$mm in water; (b) the conical cavity just before jet formation; (c) the shape contours extracted from (a) and (b) are superposed together to show bottom cavity movement.

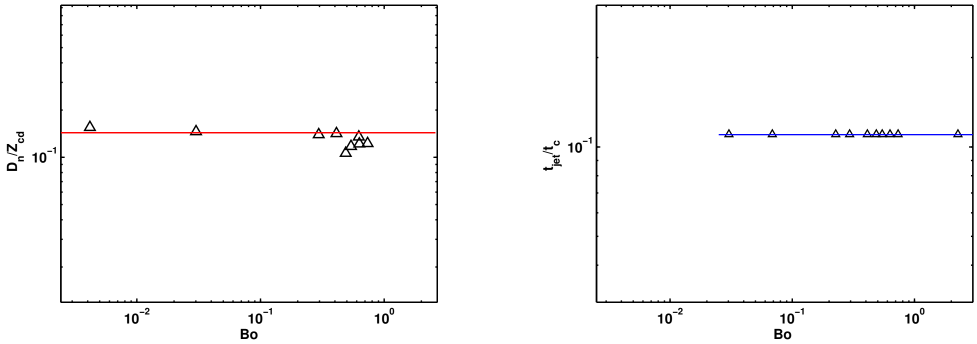

(a) (b)

Figure A.13: (a) Dimensionless $D_n = Z_{cd} - \widetilde{Z}_{cd}$ with Bo for water. $\triangle$, water; —, $D_n/Z_{cd} = 0.143$. (b) Dimensionless time versus Bo of cavity retraction from the conical shape to the jet emergence to the free surface. —, $t_{jet}/t_c = 0.11$.

Figure A.13b shows that in the intermediate range of Bo, where viscous damping of capillary waves are not significant, $C_2 = 0.11$, but at lower Bo values, corresponding to larger values of Oh, C_2 is likely to be less. We however were not able to measure at these low Bo and therefore took the same value of C_2, knowing that this would underestimate U_j. Substituting (A 2) and (A 3) in (A 1) leads to

$$We_{jc} = 60.7 \; (Z_{cd}/R)^2, \tag{A 4}$$

where We_{jc} is the Weber number based on U_{jc}. The expression for We_{jc} (A 4) has the same functional dependence as (3.10) and is quite close to (3.10) shown in figure 5. Figure A.14 compares We_{cj} determined from measured $\widetilde{Z}_{cd}$ and t_j with We determined from jet velocity measurements close to the free surface; there is a close agreement between the two. The slightly lower values of We_{cj} are due to the neglect of the initial acceleration of the jet in estimating U_{jc} since U_{jc} is an average velocity measurement over $\widetilde{Z}_{cd}$. Hence, since the time taken for the jet to travel a distance $\widetilde{Z}_{cd}$ - proportional to the cavity depth - scales as the capillary time t_c, independent of gravity effects, the gravity effects in jet velocity can only come from the gravity effects on the cavity depth.

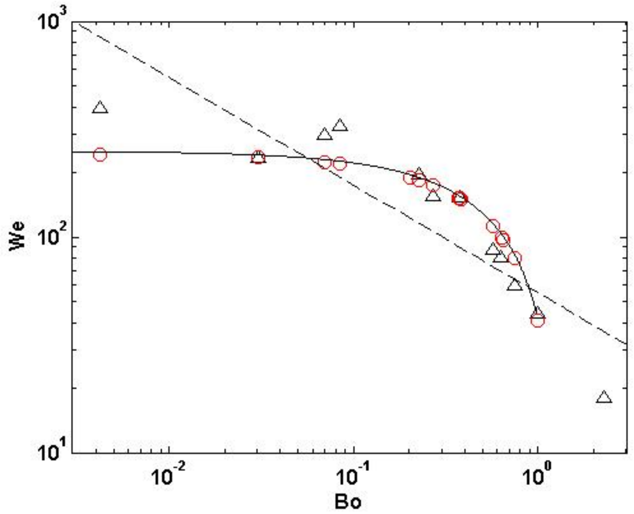

Figure A.14: Comparison of jet Weber number measured by two methods plotted against Bo. $\triangle$, We based on jet velocity at free surface; $\bigcirc$, We_{cj} based on jet velocity measured as $U_{j_c} = \widetilde{Z}_{cd}/t_j$, where $t_j = 0.11t_c$ from figure A.13b and $\widetilde{Z}_{cd} = 0.857\ Z_{cd}$; - -, $We = 55\ Bo^{-1/2}$; —, $We = 62.5(Z_{cd}/R)^2$.

Appendix B. Time evolution of jets

In Figure B.15 (a) to (d) show the time sequence of the evolution of jets and their breakup into drops with decreasing Bo and increasing Oh, while $Oh < 0.02$. Among these figures, figure B.15b shows a more detailed sequence of jet evolution for R=2.15mm in water as a continuation of figure 1. The other images, figures B.15a, B.15c and B.15d show the jet evolution issuing from collapsing bubbles in water for different Bo and Oh values. Qualitatively, it is seen that with decreasing Bo and increasing Oh the jet velocity increases, as long as $Oh < 0.02$, in agreement with figure 10. The jet diameter (d_j) is measured near the free surface when the jet just emerges. At large Bo, here at Bo=2.25 (figure B.15a), there is no jet breakup into drops, with the scaled jet diameter being $d_j/R \approx 0.32$. When Bo=0.63, figure B.15b, $d_j/R \approx 0.24$ and one drop is formed from the jet tip. In figure B.15c, Bo=0.069 the jet fragments into three droplets and $d_j/R \approx 0.25$. A further reduction in Bo, i.e, $Bo = 4.2 \times 10^{-3}$, results in a thinner jet ($d_j/R \approx 0.17$) and the entire jet gets pinched off from the surface in addition to the initial droplets shedding from the jet tip as shown in figure B.15d.

The jet size is directly related with the bubble size as seen in figure B.15 (a) to (d). However, the damping of capillary waves causes further reduction in jet size (Ghabache *et al.* (2014)) as could be seen in figure B.15d. This effect of damping on the jet size could be made clear by the jet behaviour in GWs shown in figure B.16, which shows the jet sequence with increasing Oh. Figure B.16a shows a jet from a slightly larger bubble (R=1.04mm, Bo=0.17, Oh=0.0139) compared with the jet in figure B.15c (R=0.71mm, Bo=0.069, Oh=0.0045). The jet in figure B.16a has a smaller diameter ($d_j/R \approx 0.09$) than the jet in figure B.15c ($d_j/R \approx 0.25$) due to much larger Oh. Both undergo drop shedding from the jet tip (three drops) but in figure B.16a the entire jet gets pinched off from the free surface like in figure B.15d ($d_j/R \approx 0.17$). In figures B.16b and B.16c jet evolution sequences for bubbles of approximately the same Bo values ($Bo \approx 0.1$) are

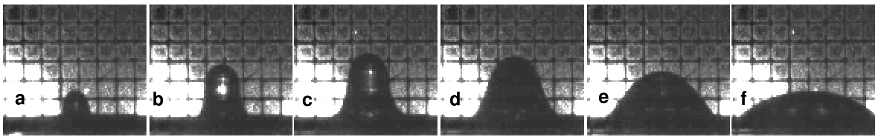

(a) $R = 4.08$mm ($Bo = 2.25$, $Oh = 1.85 \times 10^{-3}$). Each image is separated by 4ms. The grid size in the image is 1mm. $d_j/R \approx 0.32$.

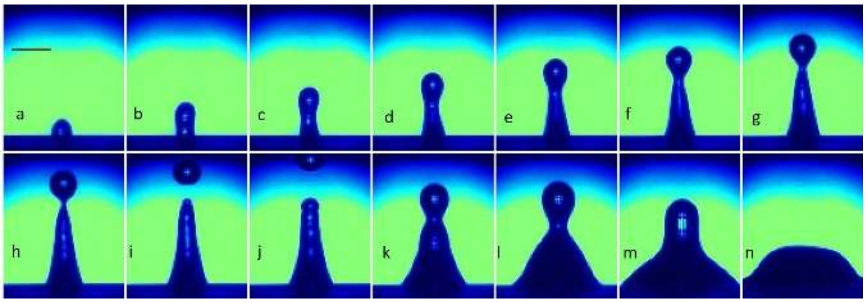

(b) $R = 2.15$mm ($Bo = 0.63$, $Oh = 2.55 \times 10^{-3}$). From a to j, each image is separated by 0.25 ms. j to k & m to n : 1.5 ms. k to l & l to m : 1.75 ms. The line in image is 1mm. $d_j/R \approx 0.24$.

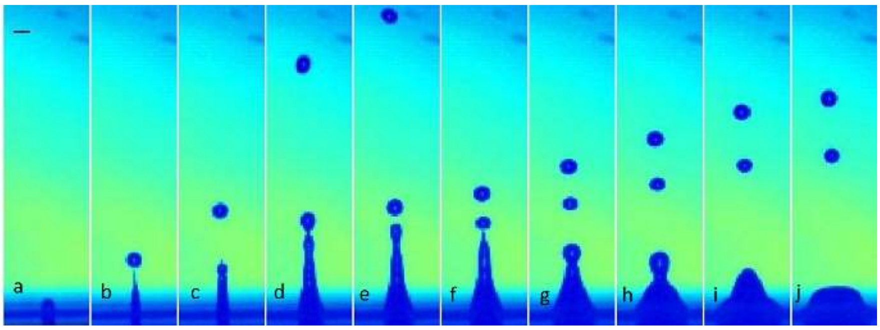

(c) $R = 0.71$mm ($Bo = 0.069$, $Oh = 4.5 \times 10^{-3}$). Time intervals: a to c , d to f & i to j: each image is separated by 0.1 ms; c to d: 0.3 ms; f to i: each image is separated by 0.2 ms. The line in image is 0.2mm. $d_j/R \approx 0.25$.

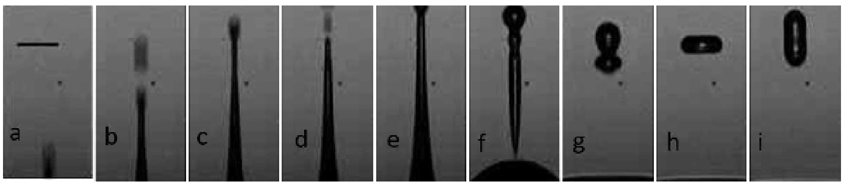

(d) $R = 0.175$mm ($Bo = 0.0042$, $Oh = 9 \times 10^{-3}$). Time intervals: a to c: each image is separated by 20μsec; c to d: 10μsec; d to e & g to h: 30μsec; e to f: 0.22ms; f to g & h to i: 60μsec; The line in image is 0.1mm. $d_j/R \approx 0.17$.

Figure B.15: Time evolution of the structure of the jet in water. Figures (a) - (d) are arranged in the order of decreasing Bo from the largest to smallest Bo of present experiments ($4.2 \times 10^{-3} \leqslant Bo \leqslant 2.25$).

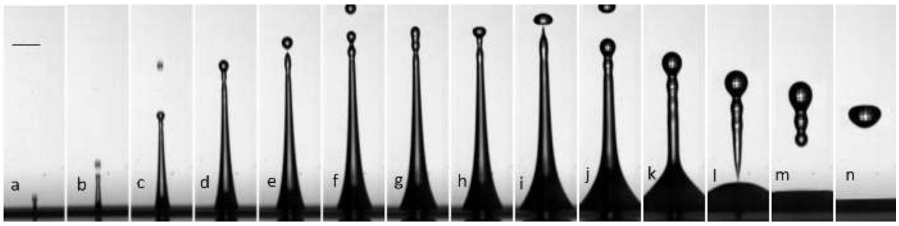

(a) $R = 1.04$mm ($Bo = 0.17$, Oh =0.0139) in GW48 (30^{o}C). Time intervals: a to b, f to g & g to h: 0.15ms; b to c, e to f & l to m: 0.44 ms; c to d: 0.52msec; d to e: 0.3msec; h to i & k to l: 0.8msec; i to j: 0.74msec; j to k & m to n: 0.96msec. The line in image is 0.5 mm. $d_j/R \approx 0.09$.

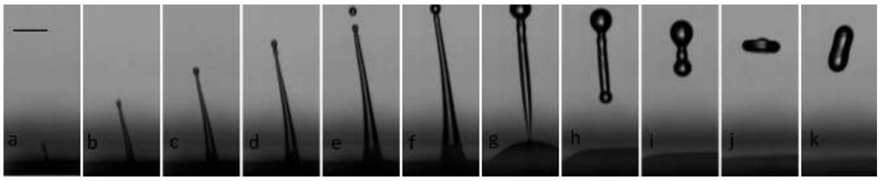

(b) $R = 0.81$mm ($Bo = 0.11$, $Oh = 2.21 \times 10^{-2}$) in GW48 (20^{o}C). Time intervals: a to d (between each images): 0.17msec; d to e: 0.27msec; e to f, g to h & h to i : 0.33msec; f to g : 2.87msec; i to j : 0.43msec; j to k: 0.83msec. The line in image is 0.5mm. $d_j/R \approx 0.04$.

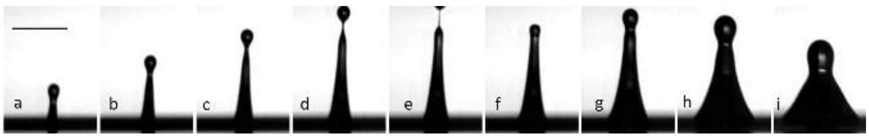

(c) $R = 0.71$mm ($Bo = 0.084$, $Oh = 3.44 \times 10^{-2}$) in GW55. Time intervals: a to d (between each images): 0.1msec; d to f (between each images): 0.05msec; f to g: 0.3msec; g to h: 0.5msec; h to i: 0.4msec. The line in image is 0.5mm. $d_j/R \approx 0.14$.

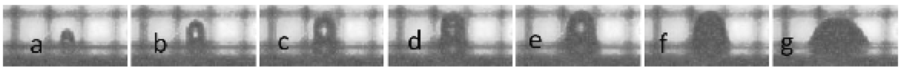

(d) $R = 1.52$mm ($Bo = 0.42$, $Oh = 4.9 \times 10^{-2}$) in GW72. Time intervals: a to f (between each images): 0.51msec; f to g: 1.54msec. Grid size is 1mm. $d_j/R \approx 0.3$

Figure B.16: Time evolution of the structure of the jet with increasing Oh in different GWs. Figures (a) to (d) are arranged in the increasing order of Oh from $Oh = 2.21 \times 10^{-2}$ in figure B.16a of GW48 (30^{0}C) to $Oh = 4.9 \times 10^{-2}$ in figure B.16d of GW72.

shown, however, the dimensionless jet radii are $d_j/R \approx 0.04$ in figure B.16b and 0.14 in figure B.16c. Only one drop is shed from the jet tip in figures B.16b and B.16c as viscosity effect become important. The jet pinched off from its base in figure B.16b as in figure B.15d and B.16a. With increase in Oh from $Oh = 2.21 \times 10^{-2}$ (figure B.16b) to $Oh = 4.9 \times 10^{-2}$ (figure B.16d), the drop pinch off is fully stopped, as discussed in §3.2 and the jet size is increased ($d_j/R \approx 0.3$).

REFERENCES

Blanchard, Duncan C 1963 The electrification of the atmosphere by particles from bubbles in the sea. *Progress in oceanography* **1**, 73IN7113–112202.

Boulton-Stone, J. M. & Blake, J. R. 1993 Gas bubbles bursting at a free surface. *Journal of Fluid Mechanics* **254**, 437–466.

Clanet, C. & Lasheras, J. C. 1999 Transition from dripping to jetting. *Journal of Fluid Mechanics* **383**, 307–326.

Das, S. P. & Hopfinger, E. J. 2008 Parametrically forced gravity waves in a circular cylinder and finite-time singularity. *Journal of Fluid Mechanics* **599**, 205–228.

Doshi, P., Cohen, I., Zhang, W. W., Siegel, M., Howell, P., Basaran, O. A. & Nagel, S. R. 2003 Persistence of memory in drop breakup: The breakdown of universality. *Science* **302** (5648), 1185–1188.

Duchemin, L., Popinet, S., Josserand, C. & Zaleski, S. 2002 Jet formation in bubbles bursting at a free surface. *Physics of Fluids (1994-present)* **14** (9), 3000–3008.

Feng, Jie, Roché, Matthieu, Vigolo, Daniele, Arnaudov, Luben N, Stoyanov, Simeon D, Gurkov, Theodor D, Tsutsumanova, Gichka G & Stone, Howard A 2014 Nanoemulsions obtained via bubble-bursting at a compound interface. *Nature physics* **10** (8), 606–612.

Ghabache, E., Antkowiak, A., Josserand, C. & Séon, T. 2014 On the physics of fizziness: How bubble bursting controls droplets ejection. *Physics of Fluids (1994-present)* **26** (12), 121701.

Joung, Y. S. & Buie, C. R. 2015 Aerosol generation by raindrop impact on soil. *Nature communications* **6**, 6083.

Kientzler, C. F., Arons, Arnold B., Blanchard, D. C. & Woodcock, A. H. 1954 Photographic investigation of the projection of droplets by bubbles bursting at a water surface1. *Tellus* **6** (1), 1–7.

Lhuissier, Henri & Villermaux, Emmanuel 2012 Bursting bubble aerosols. *Journal of Fluid Mechanics* **696**, 5–44.

Liger-Belair, G, Seon, T & Antkowiak, A 2012 Collection of collapsing bubble driven phenomena found in champagne glasses. *Bubble Science, Engineering & Technology* **4** (1), 21–34.

MacIntyre, F. 1972 Flow patterns in breaking bubbles. *Journal of Geophysical Research* **77** (27), 5211–5228.

Oguz, Hasan N. & Prosperetti, Andrea 1993 Dynamics of bubble growth and detachment from a needle. *Journal of Fluid Mechanics* **257**, 111–145.

Perlin, Marc, Lin, Huanjay & Ting, Chao-Lung 1993 On parasitic capillary waves generated by steep gravity waves: an experimental investigation with spatial and temporal measurements. *Journal of Fluid Mechanics* **255**, 597–620.

San Lee, J., Weon, B. M., Park, S. J., Je, J. H., Fezzaa, K. & Lee, Wah-Keat 2011 Size limits the formation of liquid jets during bubble bursting. *Nature communications* **2**, 367.

Sangeeth, K. & Puthenveettil, B. A. 2015 Dynamics of collapse of free surface bubbles. *Procedia IUTAM* **15**, 207–214.

Sangeeth, K., Puthenveettil, B. A. & Hopfinger, E.J. 2012 Jet formation from bubble collapse at a free surface. In *Proc. 23rd International Congress of Theoretical and Applied Mechanics, Beijing* (ed. Y. Bai, J. Wang & D. Fang), p. 171.

Shakhova, Natalia, Semiletov, Igor, Leifer, Ira, Sergienko, Valentin, Salyuk, Anatoly, Kosmach, Denis, Chernykh, Denis, Stubbs, Chris, Nicolsky, Dmitry, Tumskoy, Vladimir *et al.* 2014 Ebullition and storm-induced methane release from the east siberian arctic shelf. *Nature Geoscience* **7** (1), 64–70.

Spiel, D. E. 1995 On the births of jet drops from bubbles bursting on water surfaces. *Journal of Geophysical Research: Oceans (1978–2012)* **100** (C3), 4995–5006.

Walls, P. L. L., Henaux, L. & Bird, J. C. 2015 Jet drops from bursting bubbles: How gravity and viscosity couple to inhibit droplet production. *Physical Review E* **92**, 021002.

Woodcock, AH, Kientzler, CF, Arons, AB & Blanchard, DC 1953 Giant condensation nuclei from bursting bubbles. *Nature* **172**, 1144–1145.

Zeff, B. W., Kleber, B., Fineberg, J. & Lathrop, D. P. 2000 Singularity dynamics in curvature collapse and jet eruption on a fluid surface. *Nature* **403** (6768), 401–404.

Zhang, FH & Thoroddsen, ST 2008 Satellite generation during bubble coalescence. *Physics of Fluids (1994-present)* **20** (2), 022104.

Zhang, F. H., Thoraval, M.-J., Thoroddsen, S. T. & Taborek, P. 2015 Partial coalescence from bubbles to drops. *Journal of Fluid Mechanics* **782**, 209–239.